

# Reconstructing bifurcation behavior of a nonlinear dynamical system by introducing weak noise

Debraj Das\*

*Department of Physics, Ramakrishna Mission Vivekananda University, Belur Math, Howrah 711202, India*

Sayan Roy\*

*Department of Physics, Indian Institute of Science Education and Research Bhopal,  
Bhopal Bypass Road, Bhauri, Bhopal 462 066, Madhya Pradesh, India*

Shamik Gupta

*Department of Physics, Ramakrishna Mission Vivekananda University, Belur Math, Howrah 711202, India.*

(Dated: December 15, 2024)

For a model nonlinear dynamical system, we show how one may obtain its bifurcation behavior by introducing noise into the dynamics and then studying the resulting Langevin dynamics in the weak-noise limit. A suitable quantity to capture the bifurcation behavior in the noisy dynamics is the conditional probability to observe a microscopic configuration at one time, conditioned on the observation of a given configuration at an earlier time. For our model system, this conditional probability is studied by using two complementary approaches, the Fokker-Planck and the path-integral approach. The latter has the advantage of yielding exact closed-form expressions for the conditional probability. All our predictions are in excellent agreement with direct numerical integration of the dynamical equations of motion.

PACS numbers: 05.45.-a, 05.40.Ca, 05.10.Gg

## I. INTRODUCTION

Nonlinear dynamical systems present a plethora of physical phenomena that are truly fascinating, but which at the same time appear counterintuitive and intriguing, especially when viewed from the perspective of linear systems that are much simpler to understand and analyze [1, 2]. As examples, one may cite chaos [3], pattern formation [4], solitons [5], and many more. Despite the intricacies and roadblocks involved in providing an analytical characterization, nonlinear phenomena have attracted immensely the attention of physicists, engineers, biologists and mathematicians, a reason being that nature is inherently nonlinear.

A very interesting dynamical feature exhibited by nonlinear systems is that of bifurcation, whereby a given dynamics exhibits qualitatively different flow structure as one or more dynamical parameters are varied. A consequence is that fixed points to which the dynamical variables settle at long times may have different stability properties for different parameter ranges, or they may even be created or destroyed as the dynamical parameters are tuned across critical values.

A dynamical system is typically characterized in terms of behavior of specific initial conditions under the dynamical evolution. In contrast, introducing noise into the dynamics requires a statistical description in terms of a suitable distribution of the dynamical variables and a study of its evolution in time. In this work, we address

the issue of how one may obtain the bifurcation diagram of a nonlinear dynamical system by introducing noise into its dynamics and studying the resulting noisy dynamics using tools of stochastic processes. We show that a suitable quantity to capture the bifurcation behavior in the noisy dynamics is the conditional probability to observe a microscopic configuration of the dynamical variables at one time, conditioned on the observation of a given configuration at an earlier time. We study this conditional probability by two complementary approaches, the Fokker-Planck and the path-integral approach, with the latter offering the advantage of yielding an exact closed-form expression for the conditional probability. Our results demonstrate that when considered in the limit of weak noise, the noisy dynamics is able to reproduce faithfully the bifurcation diagram of the noiseless dynamics. Such a conclusion may not seem very surprising in retrospect, especially since in the weak-noise limit, the noisy dynamical trajectories represent small fluctuations about those for the noiseless one. Our work primarily serves as a proposal of a theoretical framework to systematically obtain the stability properties of the noiseless dynamics from a suitable analysis of the noisy one, and as an illustration of how one may derive analytical expressions of the quantities involved in the latter analysis.

The paper is laid out as follows. In Section II, we present our model system described in terms of noiseless time evolution of a single phase-like variable on a potential landscape. We discuss some of the dynamical features of the system, and also introduce its noisy variant involving time evolution in presence of Gaussian, white noise. An analysis of the bifurcation behavior of the noiseless dynamics is taken up in Section III. The

---

\* These two authors contributed equally.

noisy dynamics is studied in Section IV using two independent approaches, the Fokker-Planck and the path-integral approach. In Section V, the results obtained in the noisy dynamics in the limit of weak-noise are compared with those for the noiseless dynamics, allowing us to demonstrate how our objective of obtaining the bifurcation diagram of the noiseless dynamics from the noisy one is achieved. The paper ends with conclusions in Section VI.

## II. THE MODEL

We consider a dynamical system described by a single phase-like variable  $\theta \in [-\pi, \pi]$ , whose time evolution is given by

$$\frac{d\theta}{dt} = A \sin \theta - B \sin 2\theta. \quad (1)$$

Here, the dynamical parameters  $A$  and  $B$  are real constants. One may get rid of one of the parameters from the dynamics by a simple rescaling of time, so that from now on we will consider the dynamics

$$\frac{d\theta}{dt} = a \sin \theta - \sin 2\theta, \quad (2)$$

where  $a$  is a real constant.

The noisy dynamics corresponding to the noiseless evolution (2) is obtained by introducing a Gaussian, white noise term  $\eta(t)$  on the right hand side of Eq. (2). One has consequently the following Langevin dynamics:

$$\frac{d\theta}{dt} = a \sin \theta - \sin 2\theta + \eta(t), \quad (3)$$

where the noise  $\eta(t)$  satisfies

$$\langle \eta(t) \rangle = 0, \quad \langle \eta(t)\eta(t') \rangle = 2D\delta(t-t'), \quad (4)$$

with  $D$  a positive constant, and angular brackets denoting average over noise realizations. Note that the parameter  $D$  sets the strength of the noise, and setting it to zero reduces the noisy dynamics to the noiseless one, Eq. (2).

Equation (3) corresponds to overdamped dynamics of  $\theta$  in a potential  $V(\theta)$ , as

$$\frac{d\theta}{dt} = -V'(\theta) + \eta(t), \quad (5)$$

with

$$V(\theta) \equiv a \cos \theta - \frac{1}{2} \cos 2\theta, \quad (6)$$

and the prime denoting first derivative with respect to  $\theta$ .

Note that the potential satisfies  $V_{a<0}(\theta) = V_{a>0}(\theta - \pi)$ . Solving  $V'(\theta) = 0$  gives for all  $a$  the solutions  $\theta = 0, \pm\pi$  as well as  $\theta = \cos^{-1}(a/2)$ ,  $\sin \theta = \pm\sqrt{1 - a^2/4}$  for  $-2 < a < 2$ . It is easily checked that  $\theta = 0$  is a maximum of

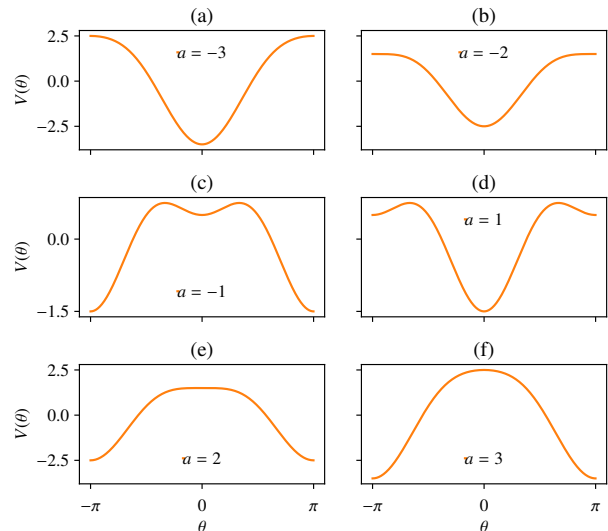


FIG. 1. (Color online) Potential  $V(\theta) = a \cos \theta - (1/2) \cos 2\theta$  for representative values of the parameter  $a$ .

$V(\theta)$  for  $a > 2$  and is a minimum for  $a < 2$ , while  $\theta = \pm\pi$  maximize  $V(\theta)$  for  $a < -2$  and minimize it for  $a > -2$ . Finally,  $\theta = \cos^{-1}(a/2)$  is a maximum for  $-2 < a < 2$ . On the other hand, we have  $V''(0) = 0$  for  $a = 2$  and  $V''(\pm\pi) = 0$  for  $a = -2$ , while  $V''(\theta = \cos^{-1}(a/2)) = 0$  for  $a = \pm 2$ . Figure 1 shows the potential  $V(\theta)$  for representative values of  $a$ .

## III. ANALYSIS OF THE NOISELESS DYNAMICS

The fixed points  $\theta^*$  of the noiseless dynamics (2) satisfy  $V'(\theta^*) = 0$ , and hence are given by  $\theta^* = 0, \pm\pi$  for all values of  $a$ , with additional fixed points  $\theta^* = \cos^{-1}(a/2)$ ,  $\sin \theta^* = \pm\sqrt{1 - a^2/4}$  for  $a$  lying in the range  $-2 < a < 2$ . The linear stability of these fixed points may be determined by substituting in Eq. (2) the expansion  $\theta = \theta^* + \Delta\theta$ , with  $|\Delta\theta|$  small, and keeping terms to linear order in  $\Delta\theta$ . One obtains

$$\frac{d\Delta\theta}{dt} = -V''(\theta^*)\Delta\theta. \quad (7)$$

It then follows that  $V''(\theta^*) > 0$  (respectively,  $V''(\theta^*) < 0$ ) makes the perturbation  $\Delta\theta$  decay (respectively, grow) exponentially in time, rendering  $\theta^*$  linearly stable (respectively, unstable). Using the properties of  $V(\theta)$  discussed earlier, we conclude that

- For  $a > 2$ , the linearly stable fixed points are  $\theta^* = \pm\pi$ , while  $\theta^* = 0$  is linearly unstable. For  $a < -2$ , the stability of these fixed points gets exchanged.
- For  $a = 2$ , the fixed point  $\theta^* = 0$  is linearly neutrally stable, while  $\theta^* = \pm\pi$  are linearly stable. For

$a = -2$ , the fixed points  $\theta^* = \pm\pi$  are linearly neutrally stable, while  $\theta^* = 0$  is linearly stable.

- For  $-2 < a < 2$ , the fixed points  $\theta^* = 0, \pm\pi$  are linearly stable, while  $\theta^* = \cos^{-1}(a/2)$ ;  $\sin\theta^* = \pm\sqrt{1 - a^2/4}$  are linearly unstable.

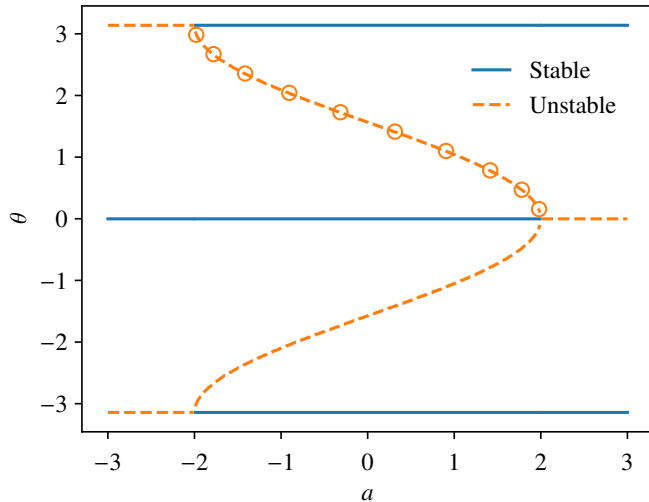


FIG. 2. (Color online) Bifurcation diagram of the noiseless dynamics (2). For all values of  $a$ , the fixed points are  $\theta = 0, \pm\pi$ , while for  $a$  in the range  $-2 < a < 2$ , additional fixed points are given by  $\cos\theta = (a/2)$ ; stable fixed points are denoted by continuous lines, while the unstable ones are denoted by broken lines. Here, the orange circles may be obtained from the exact analysis of the noisy dynamics (3) based on the Fokker-Planck and the path-integral approach discussed in the text.

On the basis of the foregoing, one obtains the bifurcation diagram of Fig. 2 that shows the stable (continuous blue lines) and unstable (broken orange lines) fixed points as a function of  $a$ . Coexistence of multiple stable fixed points for  $-2 < a < 2$  implies hysteretic behavior for the model (2). Let us identify a  $2\pi$ -periodic variable of  $\theta$  as a suitable order parameter that captures this behavior. Since the stable fixed points are either zero or  $\pm\pi$ , one may choose  $\cos\theta$  as the simplest such order parameter.

We now obtain the behavior of the stable value of  $\cos\theta$  as  $a$  is tuned adiabatically from small to large values and back. Adiabatic tuning of  $a$  ensures that the system while starting from an initial state has enough time to relax to the stable state before the value of  $a$  changes appreciably. Referring to Fig. 1, if one starts with a value of  $a$  smaller than  $-2$ , any initial  $\theta$  will relax at long times to the stable fixed point at  $\theta^* = 0$ . As  $a$  is now adiabatically tuned to higher values, the value of  $\theta$  will remain pinned to zero, until the minimum at  $\theta = 0$  of the potential  $V(\theta)$  turns into a maximum. The value of  $a$  at which this happens, obtained by solving  $V''(0) = 0$ , is given by  $a = 2$ . Beyond  $a = 2$ , the stable value of  $\theta$  will change to the value at the new minima, given by  $\theta = \pm\pi$ . Concomitant with the aforementioned behavior,

$\cos\theta$  versus  $a$  will behave as shown in Fig. 3 for the case of increasing  $a$ . Following the above line of argument, one may easily obtain the behavior of  $\cos\theta$  versus  $a$  for the case when  $a$  has a starting value greater than 2 and is adiabatically decreased to a value less than  $-2$ . The corresponding behavior is depicted in Fig. 3 for the case of decreasing  $a$ . Hysteretic behavior of  $\cos\theta$  is clearly evident from the figure.

With respect to the bifurcation diagram (2), one may wonder about the nature of bifurcation at the point ( $a = 2, \theta = 0$ ): on decreasing  $a$  across  $a = 2$ , a line of unstable fixed points bifurcates into two lines of unstable fixed points that are symmetrically disposed about a line of stable fixed points. Close to the bifurcation point, expanding Eq. (2) to the first two leading orders in  $\theta$ , one gets

$$\frac{d\theta}{dt} = (a - 2)\theta + (8 - a)\frac{\theta^3}{6}, \quad (8)$$

which has the form of the so-called subcritical pitchfork bifurcation [1]. Proceeding similarly, it is easy to see that the bifurcation that occurs as  $a$  is increased through ( $a = -2, \theta = \pm\pi$ ) is also a subcritical pitchfork bifurcation.

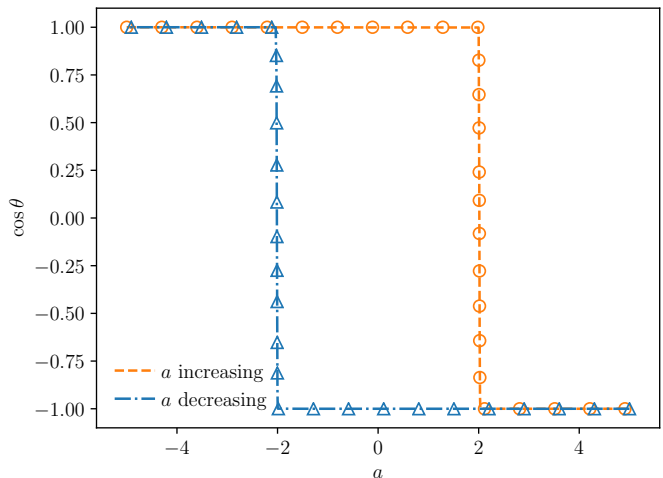


FIG. 3. (Color online)  $\cos\theta$  as a function of adiabatically-tuned  $a$ , showing hysteretic behavior. The curves follow from the linear stability analysis of the noiseless dynamics (2) discussed in the text. On the other hand, the orange circles and the blue triangles are obtained by numerically integrating the noisy dynamics (3) for the initial condition  $\theta_0 = 0.75\pi$ , and with  $D = 10^{-5}$  and time step  $dt = 10^{-3}$ ; we first let the system reach the stable state (reached at time  $t = 10$ ) at a given value of  $a < -2$ , and then increase  $a$  adiabatically to high values and back in a cycle; Here, the data correspond to one realization of the noisy dynamics.

Figure 4 shows the dynamical trajectories for the noiseless and the noisy dynamics, Eqs. (2) and (3), respectively, from which one may observe that in the weak-noise limit ( $D \rightarrow 0$ ), the trajectories for the noisy dynamics occur as small fluctuations ( $O(\sqrt{D})$ ) about those for the

noiseless dynamics. This observation makes us anticipate that it should be possible to extract the bifurcation behavior of the noiseless dynamics (2) from a suitable analysis of the noisy dynamics (3). A straightforward numerical check of this expectation is offered by performing numerical integration of the noisy dynamics (3) for small noise strength, obtaining the values of  $\langle \cos \theta \rangle$  as a function of adiabatically-tuned  $a$ , and comparing with the results of the noiseless dynamics. Figure 3 indeed shows a match between the two results. Our aim in this work is to explain this match on the basis of a theoretical analysis of the noisy dynamics. We therefore turn to such an analysis in the next section.

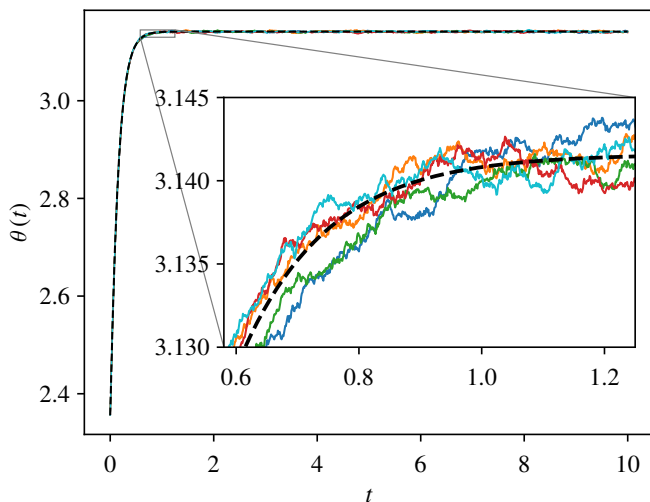


FIG. 4. (Color online) Dynamical trajectories of the noiseless and the noisy dynamics, Eqs. (2) and (3), respectively, for the initial value  $\theta_0 = 0.75\pi$ . The broken line corresponds to the noiseless case, while the five continuous lines correspond to five independent realizations of the noisy dynamics. The trajectories are obtained by numerically integrating the corresponding equation of motion with integration time step  $dt = 10^{-3}$ . Here, we have chosen  $a = 5, D = 10^{-5}$ . One may observe that the trajectories for the noisy case represent small fluctuations ( $\sim \sqrt{D}$ ) about the noiseless trajectory.

#### IV. ANALYSIS OF THE NOISY DYNAMICS

If one has to locate dynamically the stable fixed points of the noiseless dynamics (2) for a given value of  $a$ , one needs to initiate the dynamics by specifying an initial condition for  $\theta$  and then let the dynamics run for a long time in order that it relaxes to a stable state. The latter would correspond to the stable fixed points of the dynamics. In the case of noisy dynamics (3), the system while evolving from the same initial condition will have at long times a range of possible values of  $\theta$  corresponding to different dynamical trajectories attained with different realizations of the noise  $\eta(t)$ . In this case,

it is then pertinent for an analytic characterization of the dynamics that one defines a conditional probability density  $P(\theta, t|\theta_0, 0)$ , which gives the probability density that the phase has the value  $\theta$  at time  $t$ , given that it had the value  $\theta_0$  at the initial instant  $t = 0$ . Our expectation is that studying  $P(\theta, t|\theta_0, 0)$  as  $t \rightarrow \infty$  and  $D \rightarrow 0$  should allow to recover the stable fixed points of the noiseless dynamics.

The function  $P(\theta, t|\theta_0, 0)$  is  $2\pi$ -periodic in both  $\theta$  and  $\theta_0$ :

$$P(\theta + 2\pi, t|\theta_0 + 2\pi, 0) = P(\theta, t|\theta_0, 0), \quad (9)$$

and obeys the normalization

$$\int_{-\pi}^{\pi} d\theta P(\theta, t|\theta_0, 0) = 1 \quad \forall \theta_0, t. \quad (10)$$

##### A. The Fokker-Planck approach

In this subsection, we discuss how one may obtain for a given value of  $\theta_0$  the conditional probability density  $P(\theta, t|\theta_0, 0)$  as a function of  $t$  by solving the time evolution equation it satisfies. The time evolution of  $P$  is given by a Fokker-Planck equation that may be written down straightforwardly by using the Langevin equation (3). One gets

$$\frac{\partial P(\theta, t|\theta_0, 0)}{\partial t} = -\frac{\partial}{\partial \theta} [(a \sin \theta - \sin 2\theta)P(\theta, t|\theta_0, 0)] + D \frac{\partial^2 P(\theta, t|\theta_0, 0)}{\partial \theta^2}, \quad (11)$$

with the initial condition

$$P(\theta, 0|\theta_0, 0) = \delta(\theta - \theta_0). \quad (12)$$

In order to solve Eq. (11), noting that  $P$  is  $2\pi$  periodic in  $\theta$ , one may expand it in a Fourier series in  $\theta$ :

$$P(\theta, t|\theta_0, 0) = \sum_{n=-\infty}^{\infty} \tilde{P}_n(t|\theta_0, 0) e^{in\theta}. \quad (13)$$

Substituting in Eq. (11), one obtains the time evolution of the Fourier coefficients  $\tilde{P}_n$  as

$$\begin{aligned} \frac{\partial \tilde{P}_n(t|\theta_0, 0)}{\partial t} &= -Dn^2 \tilde{P}_n(t|\theta_0, 0) \\ &+ \frac{na}{2} [\tilde{P}_{n+1}(t|\theta_0, 0) - \tilde{P}_{n-1}(t|\theta_0, 0)] \\ &+ \frac{n}{2} [\tilde{P}_{n-2}(t|\theta_0, 0) - \tilde{P}_{n+2}(t|\theta_0, 0)], \end{aligned} \quad (14)$$

with Eq. (12) yielding

$$\tilde{P}_n(0|\theta_0, 0) = \frac{1}{2\pi} e^{-in\theta_0}. \quad (15)$$

For any  $n$ , the system of coupled equations (14) is not closed and in fact involves an infinite hierarchy: for a

given value of  $\theta_0$ , to obtain  $\tilde{P}_n(t|\theta_0, 0)$  as a function of  $t$  requires knowing  $\tilde{P}_{n+1}$  and  $\tilde{P}_{n+2}$  whose solution requires knowing  $\tilde{P}_{n+3}$  and  $\tilde{P}_{n+4}$ , and so on. For the initial condition (15), however, the system of equations may be solved easily by truncating it at a given value  $n = n_{\max}$ , i.e., by stipulating that  $\tilde{P}_n(t|\theta_0, 0) = 0$  for  $n > n_{\max}$  and for all  $t$ . Here,  $n_{\max}$  may be chosen to be as large as possible.

## B. The path-integral approach

We now discuss a complementary approach to obtain  $P(\theta, t|\theta_0, 0)$  as a function of  $t$ , by invoking the Feynman-Kac path-integral formalism of treating stochastic processes [6–9]. An advantage is that in contrast to the Fokker-Planck approach, one obtains in this approach a closed-form expression for  $P(\theta, t|\theta_0, 0)$ . To this end, consider a representation of the dynamics (3) in discrete times  $t_i = i\Delta t$ , with  $i = 0, 1, 2, \dots$ , and  $\Delta t > 0$  being a small time step. The discrete-time dynamics is given by

$$\theta_i = \theta_{i-1} + \Delta t (\bar{F}(\theta_i) + \eta_i), \quad (16)$$

where we have defined  $F(\theta_i) \equiv a \sin \theta_i - \sin 2\theta_i$  and  $\bar{F}(\theta_i) \equiv (F(\theta_{i-1}) + F(\theta_i))/2$ , and have used the Stratonovich rule [10] in discretizing the dynamics (3). The time-discretized Gaussian, white noise  $\eta_i$  satisfies  $\langle \eta_i \eta_j \rangle = \sigma^2 \delta_{ij}$ , where  $\sigma^2$  is a positive constant with the dimension of [time – squared]<sup>-1</sup>. In particular, the joint probability distribution of occurrence of a given realization  $\{\eta_i\}_{1 \leq i \leq N}$  of the noise, with  $N$  being a positive integer, is given by

$$P[\{\eta_i\}] = \left( \frac{1}{2\pi\sigma^2} \right)^{N/2} \exp \left( -\frac{1}{2\sigma^2} \sum_{i=1}^N \eta_i^2 \right). \quad (17)$$

From the discrete-time dynamics (16) and the joint distribution (17), the probability of occurrence of a given phase trajectory  $\{\theta_i\}_{0 \leq i \leq N} \equiv \{\theta_0, \theta_1, \theta_2, \dots, \theta_{N-1}, \theta_N = \theta\}$  is obtained as

$$P[\{\theta_i\}] = \det(\mathcal{J}) \left( \frac{1}{2\pi\sigma^2} \right)^{N/2} \times \prod_{i=1}^N \exp \left( -\frac{(\theta_i - \theta_{i-1} - \bar{F}(\theta_i)\Delta t)^2}{2\sigma^2(\Delta t)^2} \right). \quad (18)$$

Here,  $\mathcal{J}$  is the Jacobian matrix for the transformation  $\{\eta_i\} \rightarrow \{\theta_i\}$ , and is given by  $\mathcal{J}_{1 \leq i, j \leq N} \equiv (\partial \eta_i / \partial \theta_j)$ . For small  $\Delta t$ , using  $\det(\mathcal{J}) = (1/\Delta t)^N \exp \left( -\sum_{i=1}^N (\Delta t/2) F'(\theta_i) \right)$ , one gets by considering all possible trajectories that the probability density that the phase while starting at the value  $\theta_0$  at time  $t = 0$  evolves to the value  $\theta$  at time

$t = N\Delta t$  is given by [11]

$$P(\theta, t|\theta_0, 0) = \left( \frac{1}{2\pi\sigma^2(\Delta t)^2} \right)^{N/2} \prod_{i=1}^{N-1} \int_{-\pi}^{\pi} d\theta_i \times \exp \left( -\Delta t \sum_{i=1}^N \left[ \frac{[(\theta_i - \theta_{i-1} - \bar{F}(\theta_i)\Delta t)/\Delta t]^2}{2\sigma^2\Delta t} + \frac{F'(\theta_i)}{2} \right] \right). \quad (19)$$

In the limit of continuous time (i.e.,  $\Delta t \rightarrow 0$ ), using  $D \equiv \lim_{\sigma^2 \rightarrow \infty, \Delta t \rightarrow 0} (\sigma^2/2)\Delta t$ , and defining  $\mathcal{D}\theta(t) \equiv \lim_{N \rightarrow \infty} \left( 1/(4\pi D\Delta t) \right)^{N/2} \prod_{i=1}^{N-1} \int_{-\pi}^{\pi} d\theta_i$ , one gets an exact expression for the corresponding probability density to be given by the following path integral [11]:

$$P(\theta, t|\theta_0, 0) = \int_{\theta(0)=\theta_0}^{\theta(t)=\theta} \mathcal{D}\theta(t) \exp(-S[\{\theta(t)\}]), \quad (20)$$

where we have introduced the action as

$$S[\{\theta(t)\}] = \int_0^t dt \left[ \frac{[(d\theta/dt) - F(\theta)]^2}{4D} + \frac{F'(\theta)}{2} \right]. \quad (21)$$

We may now invoke the Feynman-Kac formalism to identify the path integral on the right hand side of Eq. (20) with the propagator of a quantum mechanical evolution in (negative) imaginary time due to a quantum Hamiltonian  $H_q$ . We then have

$$P(\theta, t|\theta_0, 0) = \exp \left( \frac{1}{2D} \int_{\theta_0}^{\theta} F(\theta) d\theta \right) G_q(\theta, -it|\theta_0, 0) = \mathcal{F}(\theta, \theta_0) G_q(\theta, -it|\theta_0, 0), \quad (22)$$

with

$$\mathcal{F}(\theta, \theta_0) \equiv \exp \left( \frac{1}{2D} \left[ a(\cos \theta_0 - \cos \theta) + \frac{\cos 2\theta - \cos 2\theta_0}{2} \right] \right), \quad (23)$$

$$G_q(\theta, -it|\theta_0, 0) \equiv \langle \theta | \exp(-H_q t) | \theta_0 \rangle,$$

where the quantum Hamiltonian is

$$H_q(\theta) \equiv -\frac{1}{2m_q} \frac{\partial^2}{\partial \theta^2} + V_q(\theta), \quad (24)$$

the mass in the equivalent quantum problem is

$$m_q \equiv \frac{1}{2D}, \quad (25)$$

and the quantum potential is given by

$$V_q(\theta) \equiv \frac{(F(\theta))^2}{4D} + \frac{F'(\theta)}{2} = \frac{(a \sin \theta - \sin 2\theta)^2}{4D} + \frac{a \cos \theta - 2 \cos 2\theta}{2}. \quad (26)$$

Note that in the quantum propagator in Eq. (23), the Planck's constant has been set to unity.

In terms of the eigenvalues  $E_n$  and the eigenfunctions  $\Phi_n(\theta)$  of the Hamiltonian  $H_q(\theta)$ , we have

$$G_q(\theta, -it|\theta_0, 0) = \sum_n \Phi_n(\theta)\Phi_n^*(\theta_0)e^{-E_n t}. \quad (27)$$

Hence, we have

$$P(\theta, t|\theta_0, 0) = \mathcal{F}(\theta, \theta_0) \sum_n \Phi_n(\theta)\Phi_n^*(\theta_0)e^{-E_n t}. \quad (28)$$

In the limit  $t \rightarrow \infty$ , we may expect that only the eigenvalue equal to zero (provided it exists) will matter, so that we have

$$P(\theta, t \rightarrow \infty|\theta_0, 0) = \mathcal{F}(\theta, \theta_0)\Phi_0(\theta)\Phi_0^*(\theta_0). \quad (29)$$

Equations (28) and (29) constitute our exact expressions for the conditional probability.

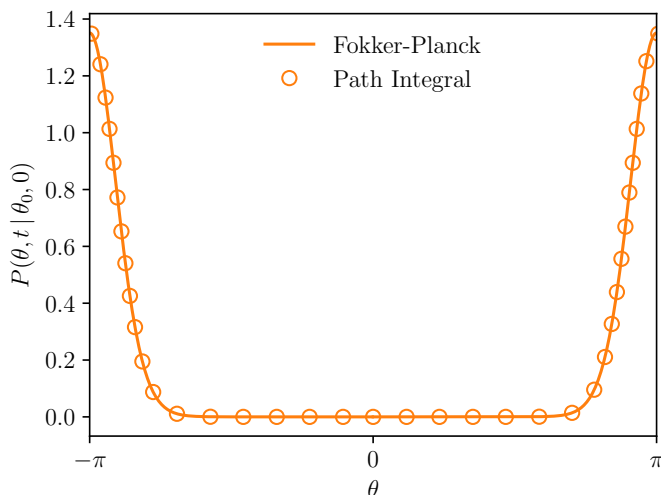


FIG. 5. (Color online) Comparison of the conditional probability  $P(\theta, t|\theta_0, 0)$  obtained from the Fokker-Planck and the path integral approach. Here, we have chosen  $a = 4$ ,  $D = 0.5$ ,  $t = 5$ ,  $\theta_0 = 0.75\pi$ . Note that the probability is peaked at  $\theta = \pm\pi$ , the stable fixed point at this value of  $a$ , see Fig. 2.

In Fig. 5, we show a comparison of the conditional probability  $P(\theta, t|\theta_0, 0)$  obtained from the Fokker-Planck and the path-integral approach, for representative values of  $a$ ,  $D$ ,  $t$  and  $\theta_0$ . In the Fokker-Planck approach, we have taken the truncation parameter to be  $n_{\max} = 60$ , making sure that higher values do not affect our results appreciably. In the path-integral approach, we obtain the eigenvalues  $E_n$  and the eigenfunctions  $\Phi_n$  of the Hamiltonian (24) by discretizing  $\theta$  over  $[-\pi, \pi]$ , expressing the Hamiltonian as a matrix and then solving numerically the corresponding eigenvalue equation. Figure 5 demonstrates an excellent agreement between the results obtained in the two approaches. From the figure, it is evident that the probability is peaked at  $\theta = \pm\pi$ , the stable fixed point at the considered value of  $a$ ; our expectation is that the density  $P(\theta, t|\theta_0, 0)$  gets more sharply peaked as  $D \rightarrow 0$ , thus allowing to recover the stable fixed points of the noiseless dynamics from the noisy one.

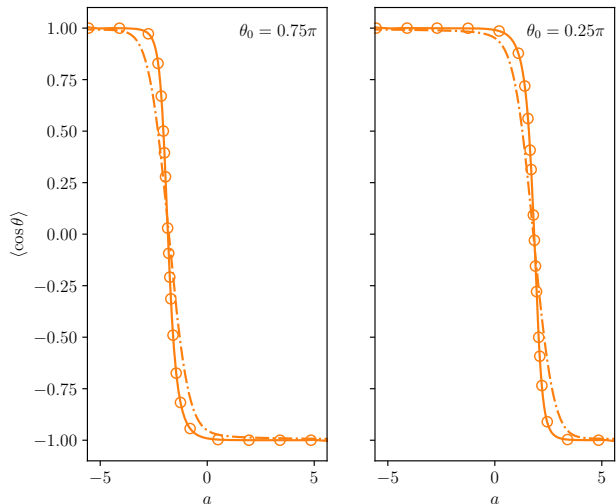


FIG. 6. (Color online)  $\langle \cos \theta \rangle$  vs.  $a$  at time  $t = 1$ , and for  $\theta_0 = 0.75\pi$  (left panel) and  $\theta_0 = 0.25\pi$  (right panel). The lines are obtained by using Eq. (30): The continuous lines are for  $D = 10^{-5}$ , while the dash-dotted lines are for  $D = 10^{-1}$ . On the other hand, the dash-circles are obtained by numerically integrating the noiseless dynamics (2) with integration time step  $dt = 10^{-3}$ . The plots show that the curves corresponding to the noiseless dynamics coincide with the noisy ones in the limit  $D \rightarrow 0$ .

## V. RESULTS AND DISCUSSIONS

We now discuss the results obtained from the analysis of the noisy dynamics (3) discussed in the preceding section. For a given initial value  $\theta_0$  and a given noise strength  $D$ , we may calculate the average of  $\cos \theta$  at a given time  $t$  and for different values of  $a$  by using either the Fokker-Planck or the path-integral result for the conditional probability density  $P(\theta, t|\theta_0, 0)$ , as

$$\langle \cos \theta \rangle \equiv \langle \cos \theta \rangle(a, D, \theta_0, t) = \int_{-\pi}^{\pi} d\theta \cos \theta P(\theta, t|\theta_0, 0). \quad (30)$$

Figure (6) shows that the results so obtained in the limit  $D \rightarrow 0$  (specifically, for  $D = 10^{-5}$ ) are in excellent agreement with the values of  $\cos \theta$  estimated from numerical integration of the noiseless dynamics (2). This is consistent with Fig. 4 showing that the noisy trajectories in the limit  $D \rightarrow 0$  represent small fluctuations about the trajectories obtained in the noiseless dynamics.

In the next step towards obtaining the bifurcation behavior of the noiseless dynamics from the noisy one, we take  $D = 10^{-5}$ , and obtain for a given  $\theta_0$  and a given time  $t$  the behavior of  $\langle \cos \theta \rangle$  versus  $a$  by using Eq. (30). It is evident from the results shown in Fig. 7 that the crossover between the two limiting values of  $\langle \cos \theta \rangle$ , namely,  $\langle \cos \theta \rangle = +1$  and  $\langle \cos \theta \rangle = -1$ , becomes steeper with the increase of  $t$ . Indeed, for larger  $t$ , one has a sharp jump,

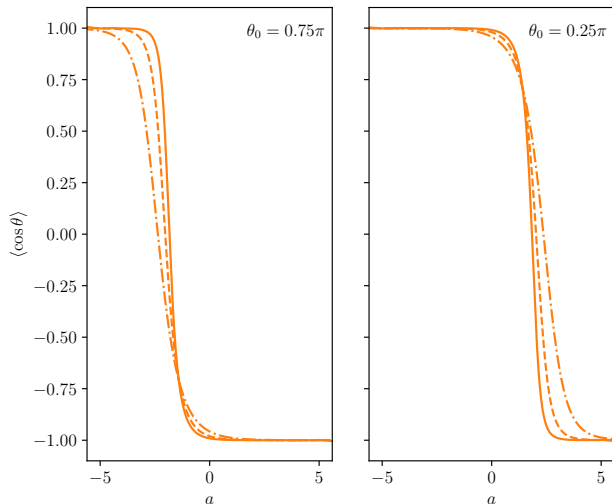


FIG. 7. (Color online)  $\langle \cos \theta \rangle$  vs.  $a$  for  $\theta_0 = 0.75\pi$  (left panel) and  $\theta_0 = 0.25\pi$  (right panel). The lines are obtained by using Eq. (30). Here, we have chosen  $D = 10^{-5}$ . The dash-dotted, the dashed and the continuous line correspond respectively to times  $t = 0.6, 0.8, 1.0$ . The plots show that the crossover between values  $\langle \cos \theta \rangle = +1$  and  $\langle \cos \theta \rangle = -1$  with change of  $a$  becomes steeper with the increase of  $t$ .

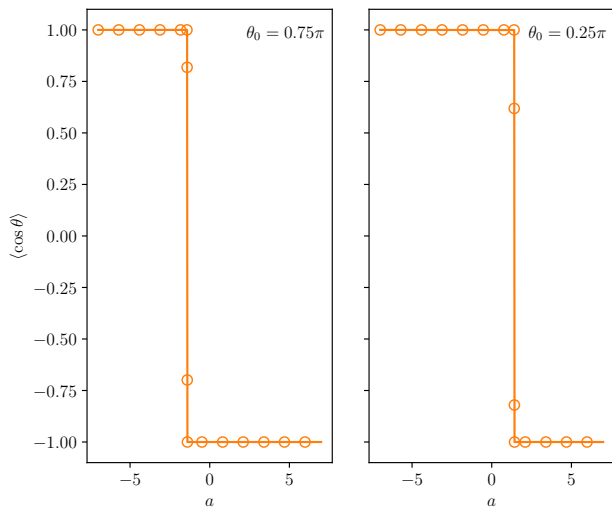


FIG. 8. (Color online)  $\langle \cos \theta \rangle$  vs.  $a$  obtained in the stable state (time  $t = 10$ ). The left panel (respectively, the right panel) corresponds to the initial condition  $\theta_0 = 0.75\pi$  (respectively,  $\theta_0 = 0.25\pi$ ). While the orange circles involve using Eq. (30), the lines are obtained from numerical integration of the noiseless dynamics (2) using integration time step  $dt = 10^{-3}$ .

as shown in Fig. 8. The same results are obtained as  $t$  is increased further, so Fig. 8 characterizes stable behavior.

In this case, we further show that the long-time values of  $\cos \theta$  obtained in the noiseless dynamics lie on the curve for the noisy dynamics.

Referring to Fig. 2, for a given  $\theta_0$ , consider increasing  $a$  from low to high values, that is, moving along a straight line parallel to the  $x$ -axis and at a distance  $\theta_0$  from it. Then, with change of  $a$ , the long-time value of  $\cos \theta$  in the noiseless dynamics will be  $+1$  so long as the straight line does not intersect the broken curve in orange lying in the region  $-2 < a < 2$ . Beyond the point of intersection, the long-time value of  $\cos \theta$  will be  $-1$ . The point of intersection, obtained by solving  $\cos \theta_0 = a/2$ , will thus be a crossover point such that for smaller (respectively, larger)  $a$ , the stable value of  $\cos \theta$  will be  $+1$  (respectively,  $-1$ ). In view of Fig. 6 showing match between the noiseless and the noisy dynamics in the limit of weak noise, such a behavior would be expected of  $\langle \cos \theta \rangle$  versus  $a$  at long times and is indeed borne out by our exact results shown in Fig. 8. It may be checked from the figure that the crossover point is obtained at the value of  $a$  given by  $a = 2 \cos \theta_0 = \pm\sqrt{2}$  for the left and the right panel, respectively. Obtaining the crossover point by repeating plots as in Fig. 8 for different values of  $\theta_0 > 0$  (those for  $\theta_0 < 0$  are obtained by symmetry) allows to obtain the line of unstable fixed points in the range  $-2 < a < 2$ . In Fig. 2, we show that as expected, the crossover points so obtained lie exactly on the unstable branch in the range  $-2 < a < 2$ . Repeating plots as in Fig. 8 for  $\theta_0 = 0$  and  $\theta_0 = \pi$  allows to obtain the crossover points  $a = 2$  and  $a = -2$ , respectively. These points coincide with the bifurcation points in Fig. 2, thereby explaining the associated stability.

## VI. CONCLUSIONS

In this work, we addressed the issue of how one may obtain the bifurcation behavior of a non-linear dynamical system by introducing noise into the dynamics and then studying the resulting Langevin dynamics in the weak-noise limit. Within the ambit of a model system, we showed that a suitable quantity to capture the bifurcation behavior in the noisy dynamics is to define a conditional probability to observe microscopic configurations at a given time while conditioned on observation of a given configuration at an earlier time. The time evolution of the conditional probability may be studied by using two complementary approaches, namely, the Fokker-Planck and the path-integral approach, with the latter yielding exact closed-form expressions for the conditional probability. A reason why we could recover the bifurcation behavior in the noisy dynamics is the choice of Gaussian noise for Langevin evolution, which ensures that typical trajectories for the noisy dynamics represent fluctuations of a given size (set by the variance  $D$  of the Gaussian distribution for the noise) around the noiseless ones, and hence coincide with the latter in the limit  $D \rightarrow 0$ . It is left for future work as to how one may

extract other features of dynamical systems by studying the corresponding noisy dynamics that allows to use standard tools of statistical physics, e.g., the Fokker-Planck and the path-integral approach.

## VII. ACKNOWLEDGEMENTS

The work of Debraj Das is supported by UGC-NET Research Fellowship Sr. No. 2121450744, dated 29-05-2015, Ref. No. 21/12/2014(ii) EU-V. Sayan Roy acknowledges DST-INSPIRE, Government of India for providing him with a scholarship to do a summer project at the Ramakrishna Mission Vivekananda University during May – July, 2018.

- 
- [1] S. H. Strogatz, *Nonlinear Dynamics And Chaos: With Applications To Physics, Biology, Chemistry, And Engineering* (Westview Press, Boulder, 2014).
  - [2] M. Lakshmanan and S. Rajaseekar, *Nonlinear Dynamics* (Springer-Verlag, Berlin, 2003).
  - [3] E. Ott, *Chaos in Dynamical Systems* (Cambridge University Press, UK, 2002).
  - [4] M. Cross and H. Greenside, *Pattern Formation and Dynamics in Nonequilibrium Systems* (Cambridge University Press, UK, 2009).
  - [5] T. Dauxois and M. Peyrard, *Physics of Solitons* (Cambridge University Press, UK, 2010).
  - [6] R. P. Feynman and A. R. Hibbs, *Quantum Mechanics and Path Integrals* (McGrawHill, New York, 2010).
  - [7] L. S. Schulman, *Techniques and Applications of Path Integration* (John Wiley and Sons, Chichester, UK, 1981).
  - [8] M. Kac, *On distribution of certain Wiener functionals*, Trans. Am. Math. Soc. **65**, 1 (1949).
  - [9] M. Kac, *On some connections between probability theory and differential and integral equations*, in *Proc. Second Berkeley Symp. Math. Stat. Prob.* (University of California Press, Berkeley, 1951).
  - [10] C. Gardiner, *Stochastic Methods* (Springer-Verlag, Berlin, 2009).
  - [11] É. Roldán and S. Gupta, *Path-integral formalism for stochastic resetting: Exactly solved examples and shortcuts to confinement*, Phys. Rev. E **96**, 022130 (2017).